Zfp503/Nlz2 Is Required for RPE Differentiation and Optic Fissure Closure

Elangovan Boobalan,[1] Amy H. Thompson,[1] Ramakrishna P. Alur,[1] David M. McGaughey,[1] Lijin Dong,[2] Grace Shih,[1] Emile R. Vieta-Ferrer,[1] Ighovie F. Onojafe,[1] Vijay K. Kalaskar,[1] Gavin Arno,[3,4] Andrew J. Lotery,[5] Bin Guan,[6] Chelsea Bender,[6] Omar Memon,[7] Lauren Brinster,[8] Clement Soleilhavoup,[9] Lia Panman,[9] Tudor C. Badea,[10–12] Andrea Minella,[13] Antonio Jacobo Lopez,[14] Sara M. Thomasy,[13,14] Ala Moshiri,[14] Delphine Blain,[1] Robert B. Hufnagel,[6] Tiziana Cogliati,[1] Kapil Bharti,[7] and Brian P. Brooks[1]

[1]Pediatric, Developmental & Genetic Ophthalmology Section, Ophthalmic Genetics & Visual Function Branch, National Eye Institute, National Institutes of Health, Bethesda, Maryland, United States
[2]Mouse Genetic Engineering Core, National Eye Institute, National Institutes of Health, Bethesda, Maryland, United States
[3]University College London Institute of Ophthalmology, London, United Kingdom
[4]Moorfields Eye Hospital, London, United Kingdom
[5]Faculty of Medicine, University of Southampton, Southampton, United Kingdom
[6]Ophthalmic Genetics Laboratory, Ophthalmic Genetics & Visual Function Branch, National Eye Institute, National Institutes of Health, Bethesda, Maryland, United States
[7]Ocular and Stem Cell Translational Research Section, Ophthalmic Genetics & Visual Function Branch, National Eye Institute, National Institutes of Health, Bethesda, Maryland, United States
[8]Division of Veterinary Resources, Office of Research Services, National Institutes of Health, Bethesda, Maryland, United States
[9]MRC Toxicology Unit, University of Cambridge, Leicester, United Kingdom
[10]Retinal Circuit Development and Genetics Unit, Neurobiology, Neurodegeneration and Repair Laboratory, National Eye Institute, National Institutes of Health, Bethesda, Maryland, United States
[11]Research and Development Institute, Transilvania University of Braşov, Braşov, Romania
[12]National Center for Brain Research, ICIA, Romanian Academy, Bucharest, România
[13]Department of Surgical and Radiological Sciences, School of Veterinary Medicine, University of California–Davis, Davis, California, United States
[14]Department of Ophthalmology and Vision Science, School of Medicine, University of California–Davis, Davis, California, United States

Correspondence: Brian P. Brooks, Ophthalmic Genetics & Visual Function Branch, National Eye Institute, Building 10/Room 10B11, 10 Center Drive, Bethesda, MD 20892, USA; brooksb@nei.nih.gov.

Received: January 24, 2022
Accepted: August 2, 2022
Published: November 3, 2022

Citation: Boobalan E, Thompson AH, Alur RP, et al. Zfp503/Nlz2 is required for RPE differentiation and optic fissure closure. *Invest Ophthalmol Vis Sci.* 2022;63(12):5. https://doi.org/10.1167/iovs.63.12.5

Purpose. Uveal coloboma is a congenital eye malformation caused by failure of the optic fissure to close in early human development. Despite significant progress in identifying genes whose regulation is important for executing this closure, mutations are detected in a minority of cases using known gene panels, implying additional genetic complexity. We have previously shown knockdown of *znf503* (the ortholog of mouse Zfp503) in zebrafish causes coloboma. Here we characterize *Zfp503* knockout (KO) mice and evaluate transcriptomic profiling of mutant versus wild-type (WT) retinal pigment epithelium (RPE)/choroid.

Methods. *Zfp503* KO mice were generated by gene targeting using homologous recombination. Embryos were characterized grossly and histologically. Patterns and level of developmentally relevant proteins/genes were examined with immunostaining/in situ hybridization. The transcriptomic profile of E11.5 KO RPE/choroid was compared to that of WT.

Results. *Zfp503* is dynamically expressed in developing mouse eyes, and loss of its expression results in uveal coloboma. KO embryos exhibit altered mRNA levels and expression patterns of several key transcription factors involved in eye development, including *Otx2*, *Mitf*, *Pax6*, *Pax2*, *Vax1*, and *Vax2*, resulting in a failure to maintain the presumptive RPE, as evidenced by reduced melanin pigmentation and its differentiation into a neural retina–like lineage. Comparison of RNA sequencing data from WT and KO E11.5 embryos demonstrated reduced expression of melanin-related genes and significant overlap with genes known to be dynamically regulated at the optic fissure.

Conclusions. These results demonstrate a critical role of *Zfp503* in maintaining RPE fate and optic fissure closure.

Keywords: Zfp503, NLZ2, coloboma, development, optic fissure

iovs.arvojournals.org | ISSN: 1552-5783

The optic fissure is a transient ventral opening along the optic cup (OC) and optic stalk (OS) during early ocular morphogenesis that permits the migration of periocular mesenchyme (Me) into the developing eye.[1,2] Proper eye development requires that the outer edges of the optic fissure, composed of a single layer of presumptive retinal pigment epithelium (pRPE) cells, approximate and fuse during the fifth to seventh weeks of human gestation, equivalent to embryonic days (E) 10.5 to 12.5 in the mouse.[3] Failure to do so results in uveal coloboma, a potentially blinding developmental eye defect in which a ventral portion of the iris, retina/retinal pigment epithelium (RPE)/choroid, and/or optic nerve does not properly form.[4] Uveal coloboma may be isolated or part of a systemic syndrome such as CHARGE (coloboma, heart anomaly, choanal atresia, retardation, genital and ear anomalies).[5,6] Mutations in more than 20 different genes have been associated with uveal coloboma. These mutations, however, account for less than 10% of cases in the absence of a clear syndromic diagnosis,[7,8] implying that additional genes and factors are involved.

We have reasoned those genes that are dynamically regulated at the edges of the optic fissure during the process of optic fissure closure are likely to be important for the execution of this developmental process.[9] Such genes, we posit, are candidates for human coloboma. We identified 168 differentially regulated genes between E10.5 and E12.5 in wild-type (WT, C57BL6/J) mice and demonstrated that morpholino knockdown in zebrafish of one such gene, *nlz2*, the ortholog of mouse *Zfp503*, results in coloboma through a *pax2*-dependent mechanism.[9,10] In mouse, *Zfp503* (*Nlz2*, *Zeppo2*, *Nolz1*, *Znf503*) mRNA is expressed throughout the OC at E10.5, becoming more limited to the area around the optic fissure by E11.5, and undetectable by in situ hybridization by E12.5.[9] Similarly, *Nlz2* mRNA is expressed at the margins of optic fissure at 24 hpf (hours post-fertilization) and is no longer detectable at 48 hpf in zebrafish.[10] Both *Zfp503* and another, closely related zinc-finger motif gene, *Zfp703* (*Nlz1*, *Znf703*, *Zeppo1*), are homologous to the *Drosophila nocA* (*no ocelli*) gene.[11] The nomenclatures of both *Zfp503* and *Zfp703* are quite heterogeneous in the literature. Indeed, the paralogues of these genes in humans, *ZNF503* and *ZNF703*, respectively, do not follow the same conventions in databases such as Ensembl and the UCSC Genome Browser (accessed October 2021). To avoid confusion, we will refer to the mouse genes by the preferred convention *Zfp503*, *Zfp703* throughout the remainder of this article. ZFP503 and ZFP703 proteins contain a single zinc finger, a Buttonhead domain, and an Sp-1–like domain and act as transcriptional repressors in most studied systems.[12–17] Although first identified in zebrafish, *Zfp503/Znf503* is widely expressed during embryogenesis in the brain, spinal cord, face, limbs, and somites of zebrafish, mice, and chicken.[12,16–22] During embryogenesis, *Zfp503/Znf503* is involved in a number of developmental processes, including motor neuron identity specification,[12] limb formation,[21] hindbrain patterning,[19] and striatal development.[20,23] *Zfp503* is also expressed in adult mammary epithelial tissue, where it downregulates E-cadherin and GATA3, promoting an aggressive cancer phenotype.[13,14]

In this study, we created a knockout (KO) mouse line ($Zfp503^{-/-}$), resulting in complete loss of the corresponding protein, to gain further mechanistic insight into the role of *Zfp503* during eye development. $Zfp503^{+/-}$ mice were viable and exhibited congenital optic nerve excavation. Optic fissure closure appeared to be complete by E12.5, as with WT embryos (data not shown). Mouse KO embryos displayed near-complete loss of melanin pigment in the pRPE and uveal coloboma with 100% penetrance. Profiling of developmentally regulated ocular transcription factors revealed downregulation of MITF and OTX2 and upregulation and/or anatomically expanded expression of PAX6, PAX2, and VSX2 proteins and *Vax1* and *Vax2* transcripts, particularly in the ventral, proximal pRPE, accompanied by an expansion of cell number. These results were confirmed and quantified at the mRNA level in pRPE of E11.5 KO and WT embryos. $Zfp503^{-/-}$ mice were never observed in born litters, likely because of lung and/or ribcage abnormalities. Gene expression profiling by RNA sequencing (RNA-seq) revealed significant downregulation of melanin pigment-related genes and changes in multiple genes known to be dynamically regulated at the closing edges of the optic fissure. Sequencing of a cohort of patients with uveal coloboma did not reveal convincing loss-of-function alleles, consistent with lack of postnatal viability in $Zfp503^{-/-}$ mice.

Materials and Methods

Generation of $Zfp503^{-/-}$ Mice

$Zfp503^{-/-}$ mice were generated by gene targeting using homologous recombination. The entire coding sequence of *Zfp503* (NM_145459.3) spanning exon 2 and exon 3 was replaced by a β-galactosidase-pGK-Neo cassette (Supplementary Fig. S1A). The targeting vector was electroporated into W4 (SV129/S6) embryonic stem (ES) cells. ES clones containing the correctly targeted DNA sequence were identified by long genomic PCR and Southern blot. ES clones were further examined by karyotyping (data not shown) and injected into blastocysts of recipient mice. Germline transmission was achieved, as evidenced by approximately 90% F1 offspring exhibiting agouti coat color. Tail DNA genotyping of the *Zfp503* WT allele was done with primers 5′-exon 2 open reading frame (ORF) (GGCCACCCAGGATTATTC) and 3′-exon 2 ORF (GCCGCCGCCGCTGTGCTTAC), and mutant allele was genotyped with primers 5′-exon 2 ORF (GGCCACCCAGGATTATTC) and 3′-β-galactosidase gene (CGGGCCTCTTCGCTATTACG). The WT band was 216 bp and the mutant band was 385 bp long. Heterozygous mice were backcrossed into C57BL/6J background for at least five generations. The floxed Neo cassette was removed by mating heterozygous *Zfp503* mice with *Zp3-Cre* mice.

Animal Husbandry

Mice were housed and maintained in a 14-hour light, 10-hour dark cycle. All experiments were conducted in accordance with the Animal Study Protocol NEI-605 approved by the National Eye Institute (NEI) Animal Care and Use Committee as well as the ARVO Statement for the Use of Animals in Ophthalmic and Vision Research. Clinical examination of the anterior segment of the eyes was performed on gently restrained awake mice using a Haag-Streit BQ slit lamp (Bell Ophthalmic Technology, Westville, NJ, USA). After pupil dilation with one drop of 1% tropicamide (Alcon Laboratories, Inc., Fort Worth, TX, USA), the posterior segment of the mouse eyes was examined with a 90-D condensing lens (Volk, Mentor, OH, USA). Fundus images were obtained using the Micron III imaging system (Phoenix Research Laboratories, CA, USA) on mice sedated with intraperitoneally injected ketamine (100 mg/mL) and xylazine

(200 mg/mL) diluted in saline. The eyes were dilated with 0.5% tropicamide (Alcon Laboratories, Fort Worth, TX, USA), 2.5% phenylephrine hydrochloride for local muscle relaxation, and 0.5% proparacaine hydrochloride for local anesthesia. Hypromellose ophthalmic demulcent solution (Gonak) was used to prevent dehydration. After imaging, mice were kept on a heating pad until they were awake. Mice were euthanized with carbon dioxide using institutional standards. For histology, eyes were dissected, fixed overnight in 10% formalin, and embedded in methacrylate for sectioning through the pupillary–optic nerve axis and staining with hematoxylin and eosin (H&E).

Immunofluorescence

Embryos were washed in PBS for 5 minutes and fixed in 4% paraformaldehyde in PBS for 0.5 to 3 hours, then washed with PBS and infiltrated with 30% sucrose overnight at 4°C. Next, they were cryopreserved in Tissue Freezing Medium (Thermo Fisher Scientific, Baltimore, MD, USA), and 16-µm cryosections were prepared with a Leica Biosystems CM3050 S cryostat (Buffalo Grove, IL). Assays were repeated multiple times as indicated in the text and figure legends on at least three independent cryosections. Indirect immunofluorescence was performed with the following antibodies: rabbit polyclonal anti-ZNF503 (Sigma-Aldrich, St. Louis, MO, USA; HPA026848, 1:1000), rabbit polyclonal anti-Pax6 (Covance, Princeton, NJ, USA; 1:1000), rabbit polyclonal anti-Pax2 (Invitrogen, Carlsbad, CA, USA; 1:500), goat polyclonal anti-OTX2 (R&D Systems, Minneapolis, MN, USA; AF1979, 1:2000), goat polyclonal anti-Chx10/Vsx2 (Santa Cruz Biotechnology, Inc., Dallas, TX, USA; SC-21690, 1:2000), rabbit polyclonal anti-MITF (Sigma-Aldrich; HPA003259, 1:500), rabbit anti-Mitf (gift from K. Bharti),[24] and Isolectin GS-IB4–Alexa Fluor–488 (Thermofisher Scientific, Carlsbad, CA, USA; I21411, 1:750). For all the antibodies used in this study, antigen unmasking was achieved by boiling the tissue sections in target retrieval solution (Agilent/Dako S1700, Santa Clara, CA, USA) for 20 minutes prior to incubation with the primary antibody. Following overnight incubation in primary antibody, sections were washed three times for 10 minutes with PBS with 0.1% Tween (PBST; Invitrogen) and incubated with Alexa Fluor–488 or 555 secondary antibodies (1:1000) along with 4′,6-diamidino-2-phenylindole (DAPI; Invitrogen; 1:1000) for 1 hour at room temperature (RT). Next, sections were washed with PBST (three times for 10 minutes) and mounted with a coverslip. To visualize hyaloid vessels and to contrast with the RPE, the tissue sections were antigen retrieved for 20 minutes and incubated with Isolectin GS-IB4–Alexa Fluor–488 (1:750) along with the rabbit anti-MITF antibody (1:500) overnight at 4°C. The sections were washed with PBST (3 × 10 minutes) and incubated with anti-rabbit Alexa Fluor–555 secondary antibody and DAPI (1:1000) for an hour at RT. The slides were washed with PBST (3 × 10 minutes) and mounted with coverslips for imaging. Images were acquired with a Zeiss LSM700-880 confocal microscopes (Carl Zeiss Microscopy, LLC, Thornwood, NY, USA), maintaining the same settings and parameters when comparing two or more groups. Details of primary antibodies used are also provided in Supplementary Table S1.

In Situ Hybridization

RNA in situ hybridization was performed using the RNAScope Assay, Multiplex Fluorescent Reagent Kit V2 (Advanced Cell Diagnostics [ACD], Newark, CA, USA). Briefly, fixed embryo cryosections were dehydrated with graded alcohols (50%, 70%, and 100%) for 5 minutes each followed by hydrogen peroxide treatment (cat. 322381; ACD) for 10 minutes at RT. The slides were then washed with distilled water and antigen retrieved with RNAScope 1× Target Retrieval Reagent in a steamer for 5 minutes. After washing with distilled water, the slides were dehydrated with 100% ethanol. The samples were then treated with RNAscope Protease III for 30 minutes at 40°C and washed with distilled water. Mouse *Vax1* (cat. 85101-C2) and *Vax2* (cat. 535091) RNAscope Target probes were mixed at a ratio of 1:50 and hybridized for 2 hours at 40°C followed by two 2-minute washes with 1× wash buffer (cat. 310091; ACD). For signal amplification, sections were incubated with Amp1 for 30 minutes at 40°C and washed twice for 2 minutes with 1× wash buffer, followed by similar treatment with Amp2 and Amp3 for 15 minutes each and washes. In the last two steps of amplification, the sections were treated first with HRP-C1 for 15 minutes at 40°C, washed twice for 2 minutes with 1× wash buffer, and incubated with Tyramide Signal Amplification (TSA) plus fluorescein (1:1500) for 30 minutes at 40°C. After rinsing twice with 1× wash buffer and blocking with HRP-blocker for 15 minutes at 40°C followed by two rinses with 1× wash buffer, the slides were similarly treated with TSA plus Cyanine 3 (1:1500). Nuclei were visualized with DAPI (cat. 310098; ACD) for 30 seconds at RT. Slides were mounted with Prolong Gold antifade mounting medium and imaged with a Zeiss LSM800 Confocal microscope (Carl Zeiss Microscopy, LLC), maintaining the same settings and parameters when comparing two or more groups.

β-Galactosidase Staining

E11.5 mouse embryos were fixed with 0.2% glutaraldehyde overnight at 4°C, followed by a 3 × 15-minute wash with Buffer A (100 mM PBS, 2 mM $MgCl_2$, 5 mM EGTA) at RT and a 2 × 10-minute wash with Buffer B (100 mM PBS, 2 mM $MgCl_2$, 0.01% sodium deoxycholate, 0.02% NP40). Color was developed in the dark by incubating the embryos with Buffer C (5 mM potassium ferricyanide, 5 mM potassium ferrocyanide, 1 mM x-Gal) at 37°C. The embryos were rinsed with PBS and imaged with a Leica M205 FA fluorescence stereo microscope (Leica Microsystems Inc.).

Skeletal Staining

Mouse embryos at E18.5 were stained with Alcian Blue 8GX (A0298; Bio Basic Canada, Inc., Markham, ON, Canada) and Alizarin Red S (SC-205998; Santa Cruz Biotechnology, Inc.) as described previously.[25] Embryos were skinned and eviscerated after fixation in 95% ethanol overnight. Three complete E18.5 skeletons were stained for each WT and *Zfp503*$^{-/-}$ sample. The arms and legs of the skeletons were removed to facilitate the visualization of the sternum. Photographs were acquired with a Leica MC190 HD digital camera.

ZFP503 Human DNA Sequencing

Patients with uveal coloboma and, when available, their first-degree relatives, were recruited and examined in the Ophthalmic Genetics Clinic of the NEI under an institutional review board–approved protocol (NCT00368004, NCT01778543, or NCT00076271, www.clinicaltrials.gov). DNA from either peripheral blood leukocytes or saliva

Investigative Ophthalmology & Visual Science

was screened for pathogenic variants in genes associated with uveal coloboma, using previously described methods and workflow.[26] Briefly, the NEXTFLEX Rapid XP DNA-Seq kit (PerkinElmer, Waltham, MA, USA) and xGen Lockdown probes (Integrated DNA Technologies, Inc., Coralville, IA, USA) were used to capture exons and other genomic regions with known or suspected pathogenic variants from a custom panel of 731 genes implicated in eye development or disease. The libraries were then sequenced on Illumina NextSeq 550 (Illumina, San Diego, CA, USA) and aligned, and variants (including copy number variations) were called, annotated, and prioritized through a custom pipeline available on GitHub (https://github.com/NIH-NEI/NGS_genotype_calling & https://github.com/NIH-NEI/variant_prioritization). The pathogenicity and effect of variants were interpreted according to the American College of Medical Genetics and Genomics (ACMGG) guidelines.[27] For the independent, phenotypically agnostic cohort, the affected individual was consented and underwent whole-genome sequencing as part of the UK 100,000 Genomes Project (UK100KGP) as previously described.[28] Both parental samples were not available for segregation analysis. The subject's sequence underwent variant interpretation using the retinal disorders virtual gene panel (version 2.21, https://panelapp.genomicsengland.co.uk/panels/307/), which failed to identify a causative genotype in any known inherited retinal degeneration genes. Loss-of-function variants in the *ZNF503* gene were interrogated in the UK1000KGP Interactive Variant Analysis (v2.0) data set, including 45,356 individual genomes. High-confidence loss-of-function variants (frameshift, nonsense, and canonical splice variants) with a minor allele frequency <0.001 in the gnomAS data set were identified in the genomes and confirmed by visualization on the individual paired-end reads using the Integrative Genomics Viewer.[29] The pathogenicity and effect of variants were interpreted according to the ACMG guidelines.[27]

RNA Sequencing

Embryos (E11.5) were harvested after euthanizing timed pregnant *Zfp503*$^{+/-}$ mice with CO_2. Eyes were enucleated and the RPE/choroidal tissues were dissected after removing the retina and lens. The RPE/choroidal tissues were stored in RNAlater (Qiagen, Germantown, MD, USA) at 4°C. Three samples per genotype (each pooled from four embryos) were lysed and total RNA was isolated using the RNAeasy mini kit (Qiagen). RNA integrity was verified on a Bioanalyzer (Agilent Technologies, Santa Clara, CA, USA), and samples with RIN 8 and greater were processed for RNA-seq by the NIH Intramural Sequencing Center.

STAR 2.4.2a was used with GRCm38 to align the RNA-seq data (https://pubmed.ncbi.nlm.nih.gov/23104886/). Counts were quantified with HTSeq 0.6.1p1 with the gencode.vM8.primary_assembly.annotation.gtf (https://pubmed.ncbi.nlm.nih.gov/25260700/). DESeq2 1.30.0 was used for RNA-seq differential analysis (https://pubmed.ncbi.nlm.nih.gov/25516281/). As predicted, relatedness of gene expression was greater within either *Zfp503*$^{+/+}$ or *Zfp503*$^{-/-}$ samples than between the two groups (Supplementary Fig. S2). Principal component analysis (PCA) analysis was performed using the base R (4.0.5) prcomp function with the rlog transformation function and the 500 most variable genes. This analysis demonstrated notable differences between the *Zfp503*$^{-/-}$ and *Zfp503*$^{+/+}$ groups, with PC1 explaining 80% of the total variance (data not shown). For differential testing, the design was set as "~condition + PCA2 + laneID," where condition is the genotype status of the mouse (e.g., *Zfp503*$^{-/-}$ or *Zfp503*$^{+/+}$) and PCA2 and sequencing laneID were covariates to be corrected for. PCA2 was used as a covariate as the separation of the samples was not related to any biological factor. The DESeq2 nbinomWaldTest was used to calculate the *P* values (https://pubmed.ncbi.nlm.nih.gov/25516281/) and the corrected *P* values were calculated with the fdrtool function (https://pubmed.ncbi.nlm.nih.gov/18441000/).

Data Availability

RNA-seq data have been deposited under GEO accession number GSE180641: https://www.ncbi.nlm.nih.gov/geo/query/acc.cgi?acc=GSE180641.

Results

ZFP503 Is Expressed in the Developing Mouse Eye

We have previously shown that *Zfp503* mRNA is expressed throughout the optic vesicle, and subsequently, it is confined to the fusing optic fissure before becoming undetectable by in situ hybridization in the developing zebrafish and mouse eye.[9] To confirm the pattern of protein expression in the developing mouse, we performed immunofluorescent labeling of coronal cryosections of WT embryos at E10.5 (open fissure), E11.5 (closing fissure), and E12.5 (closed fissure) (Fig. 1). ZFP503 expression was prominently seen in the pRPE and surface ectoderm, with qualitatively lower levels of expression in the distal optic stalk at E10.5. From E11.5 through E12.5, the pRPE and the optic stalk both showed prominent ZFP503 expression. Sagittal sections of the OC best delineate the optic fissure; these revealed that ZFP503 was expressed in the pRPE lining the optic fissure at E11.5 (panels J, K, L) and that, by E12.5, a small patch of faint expression remained in the presumptive neural retina (pNR) at the now fused margins (panels M, N, O). Variable levels of expression were observed in the local Me, especially ventral to the OC (Fig. 1). We describe Me expression as "local" and not "periocular," as there was generally a layer of Me that did not express ZFP503 immediately adjacent to the OC. In mature retina, ZFP503 expression was detectable in a subpopulation of cells in the ganglion cell layer and in cells of the inner nuclear layer, presumably a subset of amacrine cells (Supplementary Fig. S3). Notably, the labeled cells did not uniquely coincide with a number of known ganglion cell and amacrine cell subpopulations—that is, BRN3a positive (Supplementary Figs. S3A–C, 3A′ –C′, arrows pointing to double-labeled cells), ISL1 positive (Supplementary Figs. S3D–F, 3D′–F′, arrows pointing to double-labeled cells), and CALRETININ positive (Supplementary Figs. S3G–I, 3G′ –I′, arrow pointing to a single double-labeled cell).

Targeted Deletion of *Zfp503* Results in Systemic Abnormalities

To better assess the role of *Zfp503* in mouse eye development, we established the *Zfp503*$^{-/-}$ mouse line via targeted deletion of the *Zfp503* coding sequence contained in exon 2 and exon 3 (Supplementary Fig. S1A). Long-range PCR was used to confirm the presence of the recombined allele in *Zfp503*$^{+/-}$ and *Zfp503*$^{-/-}$ compared to *Zfp503*$^{+/+}$ mice (Supplementary Fig. S1B). Supplementary Figure S1C shows

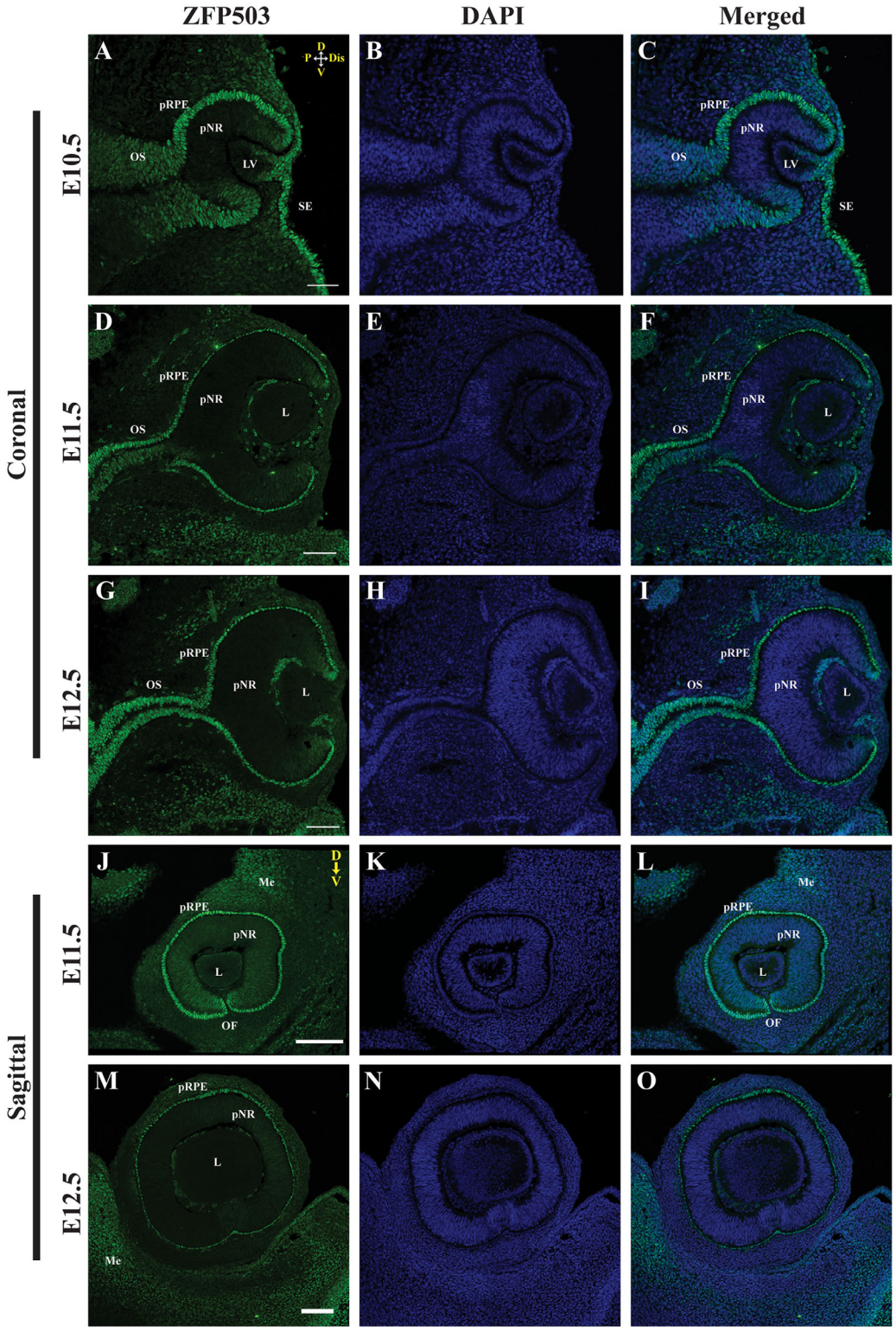

Figure 1. ZFP503 protein is expressed in the developing mouse eye. ZFP503 expression (*green*) by immunofluorescence in representative coronal (**A–I**) and sagittal (**J–O**) sections of WT mouse embryos. The three developmental time points correspond to "before closure" at E10.5, "during closure" (E11.5), and "after closure" (E12.5) of the optic fissure ($n = 3$ embryos each). DAPI nuclear staining in *blue*. Confocal microscope exposure and parameters were maintained equal for comparison purposes. Compasses in (**A**) and (**J**) apply to panels **A–I** and **J–O**, respectively: D, dorsal; Dis, distal; P, proximal; V, ventral. L, lens; LV, lens vesicle; OS, optic stalk; SE, surface ectoderm. *Scale bar*: 100 µm.

Investigative Ophthalmology & Visual Science

the corresponding PCR genotyping of tail DNA. Exon 2 and exon 3 deletion were further confirmed by RNA-seq (see below). Confocal photomicrographs of E12.5 coronal sections immunostained with anti-ZFP503 antibody showed expression in the pRPE, optic stalk, and Me in the developing eye of WT embryos (Supplementary Fig. S1D) but undetectable levels of ZFP503 in *Zfp503*$^{-/-}$ littermates (Supplementary Fig. S1E).

To establish overall *Zfp503* expression, whole E11.5 mouse embryos were stained for β-galactosidase that is expressed in *Zfp503*$^{-/-}$ mice with the same spatiotemporal pattern of the replaced *Zfp503* gene. Consistent with previous reports,[18,21–23] we observed β-galactosidase activity in the spinal cord, midbrain, eye, and limited areas of the forebrain and hindbrain of *Zfp503*$^{-/-}$ but not *Zfp503*$^{+/+}$ E11.5 embryos (Figs. 2A, 2B). No qualitative difference in the distribution and intensity of β-galactosidase activity was noted in heterozygous versus homozygous embryos (data not shown).

Zfp503$^{+/-}$ mice were viable, fertile, and without obvious systemic abnormalities or dysmorphic features (data not shown). Although their anterior segment appeared normal, dilated fundus exam and ocular histology showed abnormal pigmentation and excavation surrounding the optic nerve (Supplementary Fig. S4). Optic fissure closure was grossly complete by E12.5, as with WT embryos (data not shown). Retinal layers, including the photoreceptor and RPE, were histologically normal, albeit some abnormal layering of pigment near the optic nerve head was noted. No major dysmorphic abnormalities were visible in *Zfp503*$^{-/-}$ embryos. However, homozygous deletion of *Zfp503* resulted in neonatal lethality. Viable KO embryos were observed as late as E18.5 ($n = 39$) but were never observed at the time of weaning ($n = 555$). This observation, coupled with the broad expression pattern of *Zfp503* during development, led us to inspect several major organ systems. Histology of heart, liver, and brain was unremarkable in *Zfp503*$^{-/-}$ embryos (data not shown.) The lungs of E18.5 embryos of homozygous embryos were notably smaller ($n = 4/4$) compared to those of heterozygous/WT littermates ($n = 12$) (Figs. 2C, 2D). Histologic examination of E18.5 *Zfp503*$^{-/-}$ mice ($n = 4/4$) revealed atelectatic lungs, with reduced quantities of alveoli and bronchioles that were closer together than those of WT ($n = 4$) mice (Figs. 2E, F). The sternum was much shorter in *Zfp503*$^{-/-}$ than in WT embryos (Figs. 2G–J), with some fusion of the attached ribs (arrow). No obvious changes in rib identity, vertebrae, and limb patterning were observed in any of the mice analyzed (data not shown).

Decreased Pigmentation, Optic Fissure Closure Failure, and RPE Abnormalities in Null Mouse Eyes

Examination under the dissecting microscope showed decreased, but not completely absent, pigmentation in the pRPE of *Zfp503*$^{-/-}$ eyes compared to WT, beginning at approximately E11.5 (Figs. 3A, 3B, arrow). Additionally, while the optic fissure was fully fused at E13.5 in WT embryos (Fig. 3C), *Zfp503*$^{-/-}$ embryos had an unfused optic fissure with an opening in the ventral side of the OC (Fig. 3D, arrow). A similar phenotype was noted in *Zfp503*$^{-/-}$ embryos as late as E18.5 (data not shown), arguing against developmental delay being the cause of this finding. H&E-stained sagittal sections of WT embryos at E13.5 revealed a pigmented, smooth, and continuous pRPE, comprising a

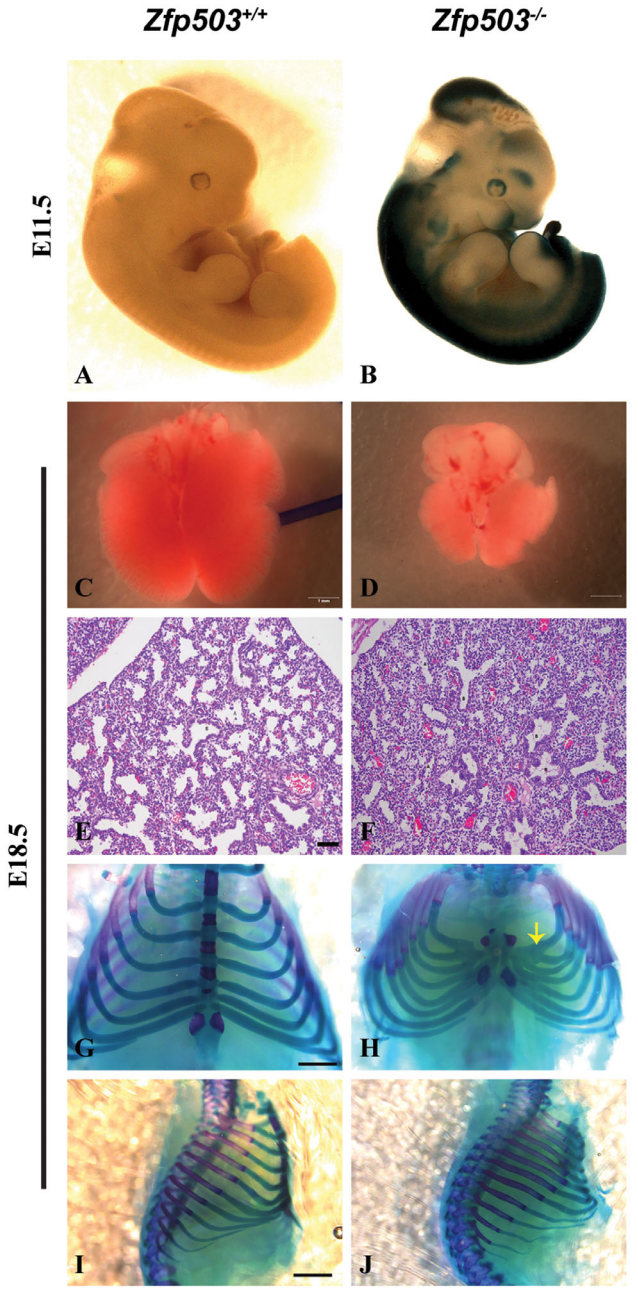

Figure 2. Homozygous deletion of *Zfp503* results in relatively normal-appearing E18.5 embryos with characteristic organ pathologies. β-Galactosidase staining (indicative of *Zfp503* localization) in representative *Zfp503*$^{-/-}$ embryos was present in the developing brain, spinal cord, eye, and branchial arches (**A**, **B**, $n = 4$/genotype). Loss of ZFP503 resulted in smaller lungs (**C**, **D**, $n = 4/4$ from two litters) and faulty alveolar formation in the lung (**E**, **F**, $n = 3$ sections through each of four embryos) visualized by H&E staining in representative histology sections. The sternum of *Zfp503*$^{-/-}$ embryos visualized with Alcian blue was shorter than in WT embryos, accompanied by abnormal rib morphology (**G**, **H**, frontal view, arrow, $n = 3$/genotype) and (**I**, **J**, lateral view). *Scale bars*: 1 mm (**C**, **D**), 50 µm (**E**, **F**), and 0.9 mm (**G–J**).

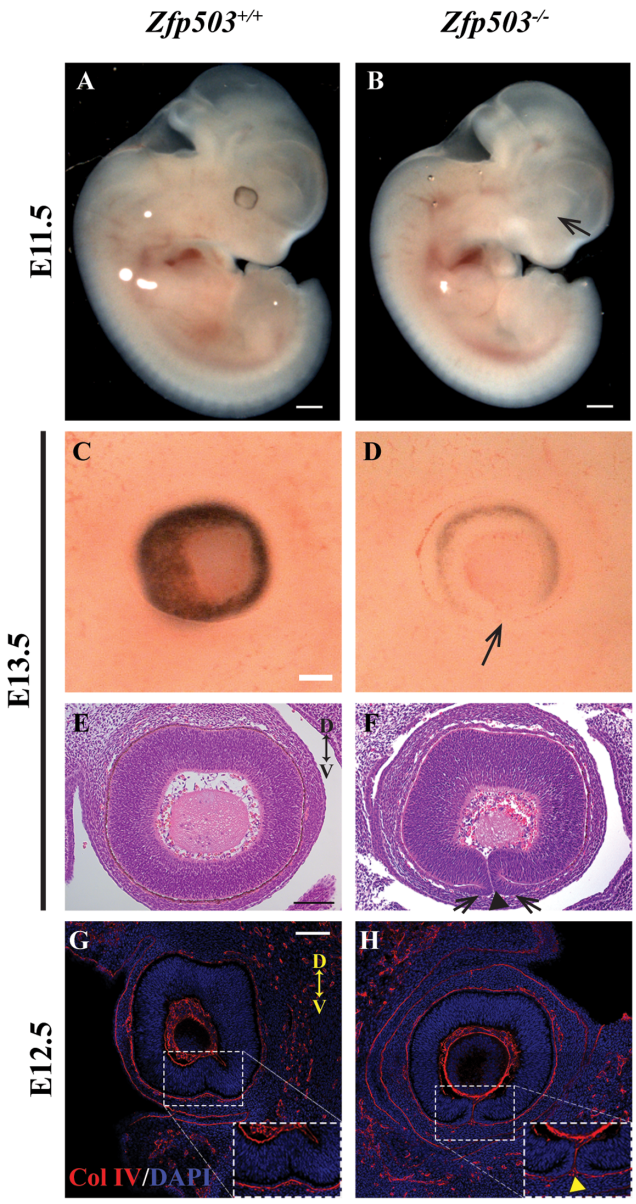

Figure 3. *Zfp503* deletion results in hypopigmentation of the RPE and uveal coloboma. Photomicrographs of representative WT embryos at E11.5 (**A**) and E13.5 (**C**) showed normal, circumferential, and continuous pigmentation of the RPE that was almost completely absent in age-matched *Zfp503*$^{-/-}$ embryos (**B**, **D**, arrows, n = 5/genotype). Sagittal sections of representative E13.5 embryos stained with H&E revealed that the edges of the optic fissure were fused and no longer discernible in WT embryos (**E**), whereas representative *Zfp503*$^{-/-}$ embryos showed distinct nonfusion of fissure edges (**F**, *arrowhead*). Note the hyperplasia, resembling pNR, flanking the fissure (*arrows*). Whereas the basement membrane of the optic fissure edges was no longer detectable by collagen IV immunostaining (*red*) in E13.5 WT embryos (**G**), a clear separation of the optic fissure edges could be seen in *Zfp503*$^{-/-}$ littermates (**H**, *arrowhead*, n = 2/genotype). DAPI nuclear staining in *blue*. Confocal microscope exposure and parameters were maintained equal for comparison purposes. Compass in (**E**, **G**) applies to **E–H**: D, dorsal; V, ventral. *Scale bars*: 500 µm (**A**, **B**); 100 µm (**C–H**).

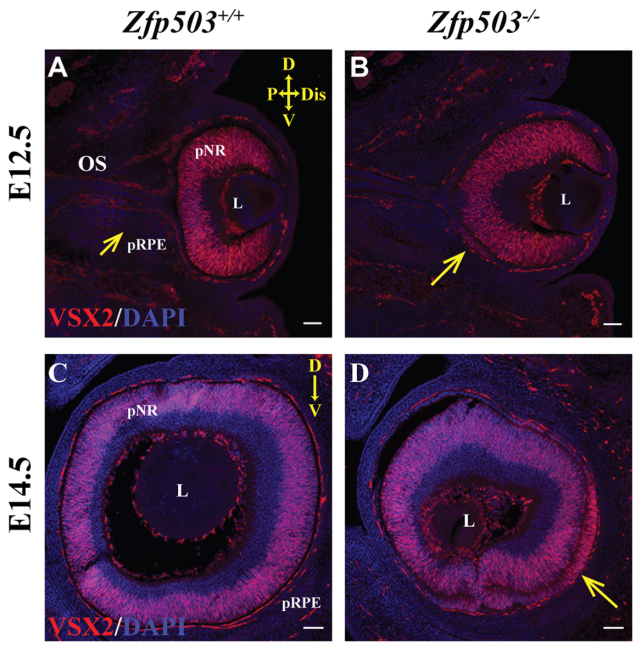

Figure 4. VSX2-positive cellular hyperplasia is observed in the pRPE of *Zfp503*$^{-/-}$ developing eyes. VSX2/CHX10 immunostaining in representative coronal sections of E12.5 WT (**A**) and *Zfp503*$^{-/-}$ embryos (**B**) demonstrates fluorescent signal (*red*) in a hyperplastic ventro-proximal population of KO pRPE (*arrow*), as well as in the pNR (as expected) in both genotypes (n = 2/genotype). By E14.5, this VSX2-positive hyperplasia extends further distally and temporally (*arrow*, **D**) in KO embryos and is absent in WT embryos (**C**) (n = 2/genotype, coronal sections). DAPI nuclear staining in *blue*. Confocal microscope exposure and parameters were maintained equal for comparison purposes. Compass in (**A**) applies to **A** and **B**, in (**C**) applies to **C** and **D**: D, dorsal; Dis, distal; P, proximal; V, ventral. L, lens; OS, optic stalk. *Scale bars*: 100 µm (**A–D**); 200 µm (**E**, **F**).

single layer of cells clearly delineated from surrounding tissue (Fig. 3E). The location of the optic fissure was no longer apparent. In *Zfp503*$^{-/-}$ sagittal sections, the pRPE lacked pigmentation throughout and multiple layers of cells resembling pNR were observed near the ventral optic fissure (Fig. 3F, arrows). Furthermore, the optic fissure failed to close, resulting in a thin but clear division between the temporal and nasal halves of the OC (arrowhead). Collagen IV staining of the basement membrane confirmed that fissure closure occurred in E13.5 WT embryos (Fig. 3G) but that separation remained in *Zfp503*$^{-/-}$ mutants (Fig. 3H). The hyaloid vasculature is normally transmitted through the optic fissure and excluded with its closure and may be important in mediating this developmental process.[30,31] Isolectin B4, a marker for the hyaloid vasculature, is not present between the closing optic fissure (OF) margins of WT embryos at E11.5 but is present in KO littermates (Supplementary Fig. S5, arrows). Whether a persistent hyaloid is a cause of coloboma (presumably through mechanically blocking fusion) or simply a marker of an unfused fissure is not clear. Nonetheless, it further underscores the coloboma phenotype in mutant embryos. The hyperplasia of the pRPE abnormally expressed the pNR marker VSX2/CHX10 and could be observed as early as E12.5 (Figs. 4A, 4B). This phenotype begins mostly ventrally and proximally at this time and is best appreciated on coronal sections. The pNR phenotype became more prominent

Investigative Ophthalmology & Visual Science

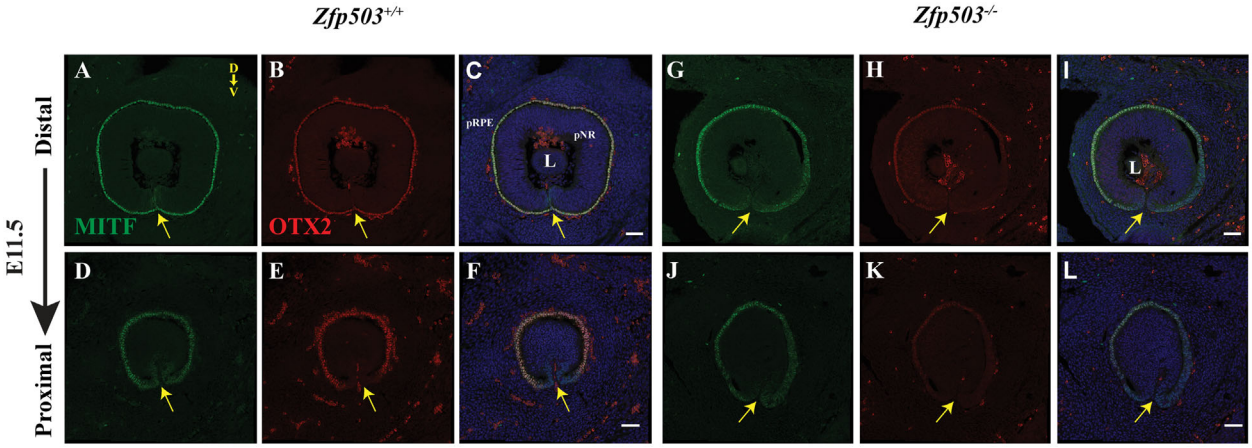

Figure 5. Loss of *Zfp503* is associated with reduced expression of MITF and OTX2. Sagittal sections from representative E11.5 WT (**A**, **B**, **D**, **E**) and *Zfp503*$^{-/-}$ (**G**, **H**, **J**, **K**) embryos immunostained with anti-MITF antibody (*green*) and anti-OTX2 are shown in distal to proximal series. Note the open optic fissure (*arrow*) in *Zfp503*$^{-/-}$ section (**I**). Qualitative reduction of MITF expression in *Zfp503*$^{-/-}$ was particularly evident in proximal sections, near the optic stalk (**L**, *arrow*). All panels were imaged with the same exposure (n = 3/genotype). Compass in (**A**) refers to all panels: D, dorsal; V, ventral. L, lens. *Scale bar*: 50 µm.

with time and extended further in the temporal region by E14.5 (Figs. 4C, 4D, arrow), best seen on sagittal sections.

Targeted Deletion of *ZFP503* Results in Abnormal Patterns of Transcription Factor Expression During Eye Development

Differentiation and maintenance of RPE involve a complex interplay of transcription factors and signaling molecules, including MITF, OTX2, VSX2, PAX6, VAX1, VAX2, WNTs, FGFs, and JAGGED-NOTCH signaling.[32–38] Therefore, to investigate the mechanism by which *Zfp503*$^{-/-}$ ocular phenotypes occur, we performed immunostaining for several key developmental markers on cryosections of WT and *Zfp503*$^{-/-}$ embryos at E11.5, the time when fissure fusion is in progress. As expected, ZFP503 was expressed in the pRPE, and VSX2 was expressed in the pNR in WT mice (Supplementary Fig. S6). Although ZFP503 expression was not detected in KO embryos, VSX2 expression was largely unchanged. Note that the hyperplasia and VSX2 expression noted at E12.5 in the ventral-proximal OC is not prominent at this time point. pRPE is also frequently identified molecularly by early expression of the transcription factors MITF and OTX2.[39–42] In E11.5 WT embryos, both MITF and OTX2 were expressed uniformly and in a nearly identical pattern along the dorsoventral axis in the pRPE (Figs. 5A–F). By contrast, MITF and OTX2 immunofluorescence was faint in the proximal OC in *Zfp503*$^{-/-}$ embryos (Figs. 5J–L). Expression of MITF and OTX2 in KO embryos appeared to increase more distally yet remained relatively reduced compared to WT in the ventral-most portion of the pRPE near the optic fissure (Figs. 5G–I). By E12.5 and E14.5, OTX2 expression in the pRPE was more noticeably decreased in KO compared to WT (Supplementary Figs. S7A–F). OTX2 is also expressed in a subset of neuroblasts and labeled the population of hyperplastic pNR-like pRPE (Supplementary Fig. S7D, arrow). Taken together, these observations suggest that *Zfp503* is not required for initial specification of the OC's outer layer of neuroepithelium into a pRPE-like monolayer of cells but is required for sustaining/advancing pRPE identity and the closure of the optic fissure soon after OC formation.

The homeobox transcription factor PAX6 also participates in RPE differentiation in concert with MITF and the transcription factor PAX2.[34,43] Consistent with previous reports, PAX2 immunofluorescence was most prominent in the ventral/proximal OC and the optic stalk, reducing more distally with only a small patch of ventral expression at E11.5 (Figs. 6A, 6D, 6G, arrows); KO embryos demonstrated dorsal expansion of staining, particularly mid-proximally (Figs. 6J, 6M, 6P). At this same time, PAX6 was expressed predominantly in the NR proximally/dorsally and gradually increased expression more distally, including expression in the pRPE and the lens vesicle (Figs. 6B, 6E, 6H); in KO mice, expression in the pRPE extended more proximally, while maintaining expression in the pNR and lens vesicle (Figs. 6K, 6N, 6Q). While PAX6 levels were low at the optic fissure margin (Figs. 6B, 6E, 6H, arrowheads) in the WT, its levels increased along with the PAX2 (Figs. 6J, 6M, 6P) in the KO. At E11.5, PAX2 and PAX6 have limited overlap in their expression domains, whereas KO embryos show greater admixture of signal, particularly proximally (Figs. 6C, 6F, 6I and 6L, 6O, 6R, respectively). At E12.5 and E14.5, the expression domains of PAX2 and PAX6 were similar to that at E11.5 in WT embryos, although with even less overlap in their domains (Supplementary Figs. S7G, 7I, 7K and 7M, 7O, 7Q). In KO embryos, however, we observed expansion of PAX2 more distally and PAX6 more proximally in the ventral pRPE. This was particularly notable in the outer, hyperplastic area of the pRPE (Supplementary Figs. S7H, 7J, 7L and 7N, 7P, 7R).

Lastly, *Vax1* expression in WT embryo eyes was present in the proximal most pRPE cells within the fissure, as well as in the ventral optic stalk at E11.5 (Figs. 7A, 7D, 7G, 7J). In *Zfp503*$^{-/-}$ eyes, *Vax1* domain was expanded into the dorsal optic stalk (data not shown) and the ventral and dorsal proximal pRPE and pNR (Figs. 7M, 7P, 7S, 7V; data not shown). *Vax2* expression at E11.5 was strongest in the ventral retinal neuroblasts, with qualitatively less intense expression in the pRPE (Figs. 7B, 7E, 7H, 7K).[44] *Vax2* was largely absent in the optic stalk. In *Zfp503*$^{-/-}$, *Vax2* expression was simi-

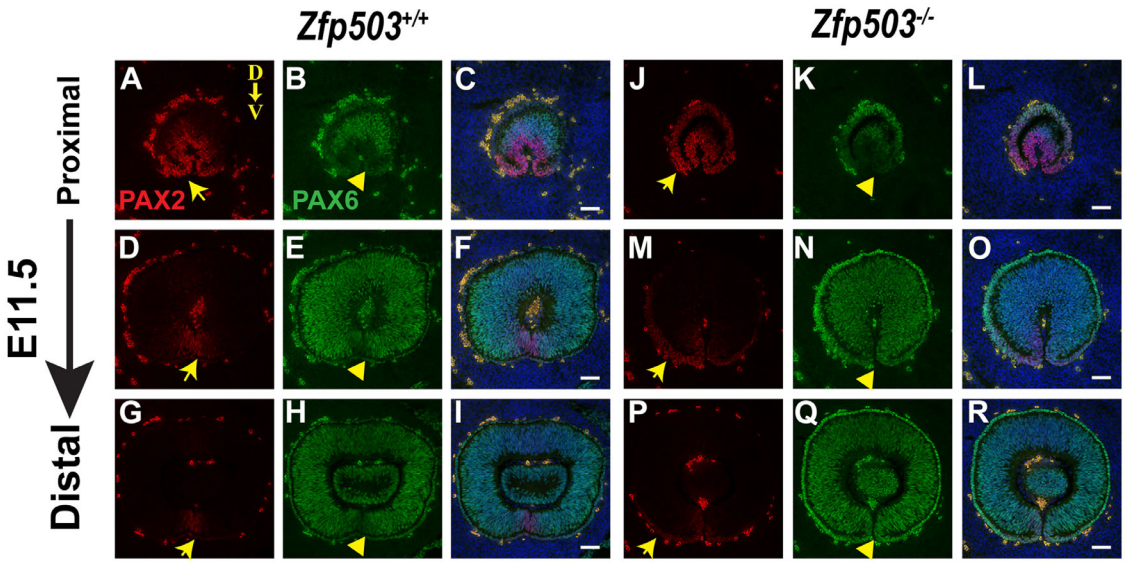

Figure 6. Loss of *Zfp503* expression is associated with an abnormal expression pattern of transcription factors important for RPE differentiation. Immunofluorescence staining for PAX2 (red) and PAX6 (green) of representative E11.5 sagittal sections of WT (**A**, **D**, **G** and **B**, **E**, **H**) and $Zfp503^{-/-}$ (**J**, **M**, **P** and **K**, **N**, **Q**) eyes are shown. PAX6 expression was increased and expanded into the proximal/dorsal pRPE of $Zfp503^{-/-}$ eyes (compare **K**, **N**, **Q** with **B**, **E**, **H**, *arrowhead*). PAX2 expression in $Zfp503^{-/-}$ eyes extended dorsally and distally into the ventral pRPE (compare **J**, **M**, **P** with **A**, **D**, **G**, *arrow*). DAPI nuclear staining in *blue*. Confocal microscope exposure and parameters were maintained equal for comparison purposes. Compass in (**A**) applies to all the panels. D, dorsal; V, ventral. L, lens; OS, optic stalk. *Scale bars*: 50 µm (n = 3/genotype).

lar to WT in the ventral pNR but appeared increased in the ventral pRPE and the proximal-most portion of dorsal pRPE (Figs. 7N, 7Q, 7T, 7W; data not shown). While the expression domains of *Vax1* and *Vax2* showed some overlap in WT embryos (Figs. 7C, 7F, 7I, 7L), this was more prominent in $Zfp503^{-/-}$ embryos (Figs. 7O, 7R, 7U, 7X). These data suggest that $Zfp503^{-/-}$ embryos have significantly expanded domains for both these transcription factors, which partially resembles patterns of overlapping expression normally seen earlier in development.

RNA-seq Confirms RPE Dysgenesis in $Zfp503^{-/-}$ Mice

To better understand the pathogenesis of coloboma in our model, we performed RNA-seq on pRPE/choroid dissected from E11.5 WT and $Zfp503^{-/-}$ embryos. A total of 148 genes were significantly upregulated in *Zfp503* KO embryos compared to WT ($\log_2$ fold change >1); by contrast, 343 genes were significantly downregulated using the same criteria (Supplementary Tables S2 and S3). Changes in *Mitf*, *Otx2*, *Pax2*, *Pax6*, *Vax1*, *Vax2*, and *Vsx2* levels (Fig. 8A) were consistent with the qualitative results we observed using immunofluorescence/in situ hybridization and were confirmed using quantitative real-time PCR on independently dissected E11.5 pRPE (data not shown). The apparent residual expression of *Zfp503* in the KO (last panel in Fig. 8A) reflected accumulation of untranslated sequencing reads in exon 1 and the untranslated region (UTR) regions flanking exons 2 and 3. As expected, the DNA regions corresponding to the deleted exons 2 and 3 that code for protein were completely devoid of any reads (Supplementary Fig. S8). A volcano plot of $\log_{10}$(P value) versus $\log_2$(fold change) is shown in Figure 8B. Consistent with the hypopigmentation observed in the pRPE, multiple genes directly or indirectly involved in melanin production/melanosome biogenesis were significantly downregulated (e.g., *Tyr*, *Dct*, *Slc45a2*, *Slc24a5*, *Gpnmb*, *Pmel*, *Gpr143*, *Mlana*, *Mlph*). Similarly, several RPE signature genes (Supplementary Table S4)[45] were significantly downregulated ($<9.5 \times 10^{-15}$, hypergeometric testing), consistent with a defect in maintaining RPE fate. A number of differentially expressed genes overlapped with those we previously identified by molecular profiling of optic fissure closure[9] ($P < 3.2 \times 10^{-9}$, hypergeometric testing), including *Strmn4*, *Insm1*, *Itgb8*, *Dcc*, *Tox3*, *Atoh7*, *Ascl1*, *Dkk3*, *Myb*, *Hes5*, *Fgf15*, and *Onecut1* (Supplementary Tables S2, S3). We note that the four most upregulated annotated genes in KO embryos involve neural development, including *Dbx1* (important for anterior brain development),[46] *Onecut1* (regulates the formation of the four early born retinal cell types),[47] *Nrn1* (promotes retinal ganglion cell survival and axon regeneration),[48] and *Scrt2* (important in cortical neurogenesis).[49] These findings are consistent with the expanded NR-like cells observed in these embryos. GO term analysis further highlights this finding, as the top three terms include "synapse organization," "axon development," and "axonogenesis" (Supplementary Fig. S9A). A "CNET" plot of relationships between related GO terms with shared genes further emphasizes this point (Supplementary Fig. S9B). Lastly, we note that several genes known to be important in eye development are among the differentially expressed pRPE genes, including *Otx2* (mutated in syndromic microphthalmia, MCOPS5, OMIM#610125),[50] *Atoh7* (mutated in autosomal recessive persistent hyperplastic primary vitreous, OMIM#221900),[51] *Indian hedgehog* (*Ihh*, required for scleral and RPE development in mouse),[52] *Sox7* (important in retinal vasculature development),[53] and *Sox21* (important in lens development).[54]

Investigative Ophthalmology & Visual Science

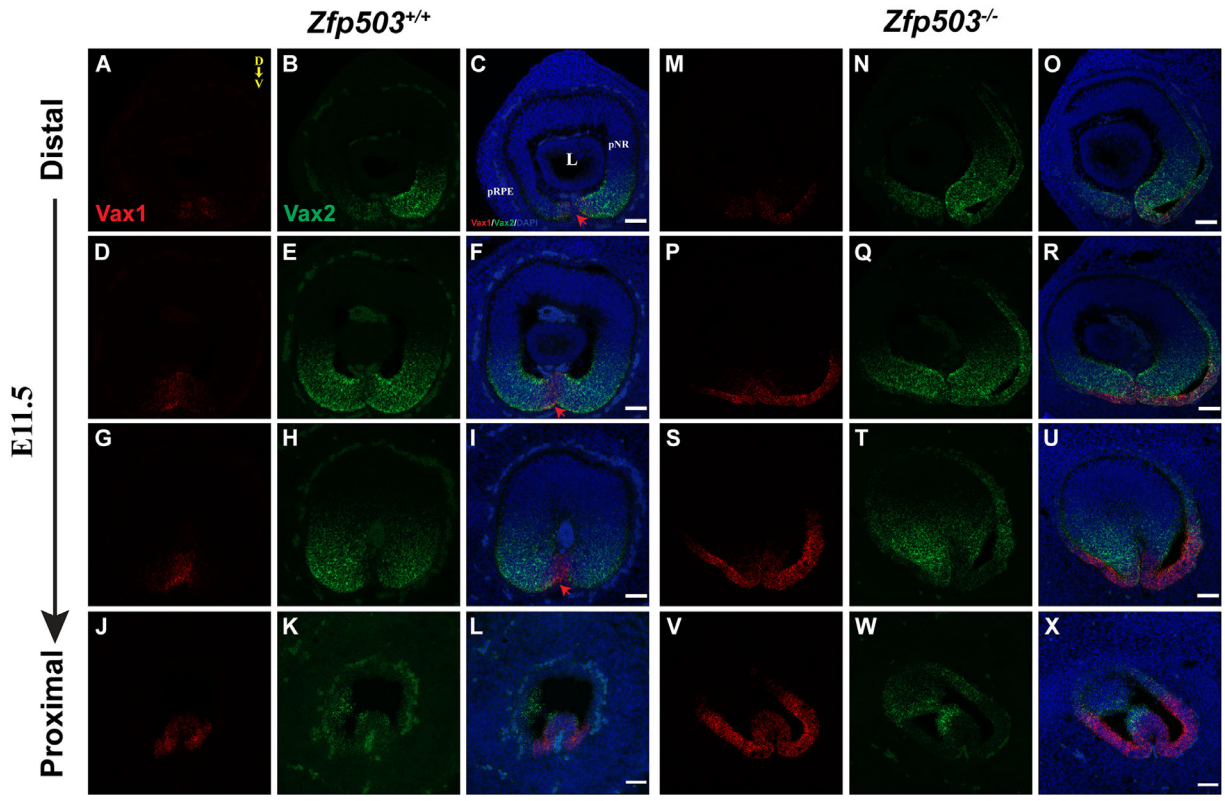

Figure 7. Loss of *Zfp503* is associated with abnormal *Vax1* and *Vax2* mRNA expression at E11.5. Microphotographs of representative sagittal section series, distal to proximal, of developing mouse eyes at E11.5 showing *Vax1* (*red*, **A**, **D**, **G**, **J**, **M**, **P**, **S**, **V**) and *Vax2* (*green*, **B**, **E**, **H**, **K**, **N**, **Q**, **T**, **W**) expression using in situ hybridization. Overlays are shown in **C**, **F**, **I**, **L**, **O**, **R**, **U**, and **X** with DAPI nuclear staining in *blue*. In WT eyes, *Vax1* expression was limited to the very proximal ventral optic cup and the ventral optic stalk (**A**, **D**, **G**, **J**), while *Vax2* signal was mostly in the ventral retinal neuroblasts of the optic cup (**B**, **E**, **H**, **K**). In *Zfp503*$^{-/-}$ embryos, *Vax1* in situ hybridization extended more dorsally and further into the proximal optic cup (**M**, **P**, **S**, **V**). *Vax2* expression was more prominent in ventral pRPE in addition to retinal neuroblasts and extended further into the optic stalk in KO embryos (**N**, **Q**, **T**, **W**). The images are from a single plane (n = 2/genotype). Confocal microscope exposure and parameters were maintained equal for comparison purposes. Compass in (**A**) is applies to all panels. D, dorsal; V, ventral. *Scale bar*: 50 µm.

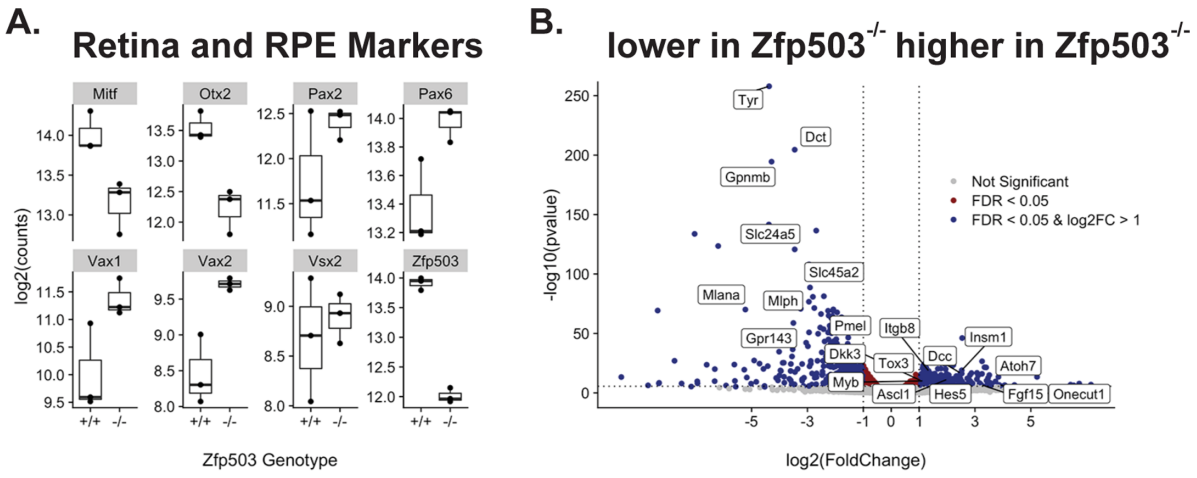

Figure 8. RNA-seq from RPE at E11.5. Quantitation of several key RPE and retina mRNA transcripts in *Zfp503*$^{-/-}$ versus *Zfp50*$^{+/+}$ embryos demonstrated changes consistent with the qualitative differences noted in immunofluorescence experiments (**A**). Volcano plot of differentially regulated genes showing changes in several key transcription factor, melanin pigmentation, and genes previously identified as changing during the time of optic fissure closure (**B**).

Table. Heterozygous *ZFP503* Variants Identified

Family	Variant*	Protein	Phenotype	Notes
98	c.697G>C	p. Ala233Pro	Morning glory anomaly OS. Normal brain MRI/MRA, spine x-ray, kidney ultrasound, echocardiogram	Missense; rs = 200297480; AF = 4.9E-4; S = Tol; PP = PosD; CADD = 26.1. Variant also found in unaffected mother
107	c.666C>G	p. Phe222Leu	Colobomatous microphthalmia OS; PSC OU; hemifacial microsomia; hypomelanosis of skin scoliosis	Missense; rs747667090, AF = 4.5E-0.5; S = Tol; PP = PrD; CADD = 25.6. Somatic trisomy 20 identified on skin biopsy of hypomelanotic lesion. Variant also found in father, who was phenotypically normal by history (unavailable for examination)
UK	c.70G>T	p. Gly24Ter	Rod-cone degeneration, cystoid macular edema, Bochdalek hernia	Not in gnomAD

AF, allele frequency in gnomAD database; CADD, combined annotation dependent depletion; MRA, magnetic resonance angiography; MRI, magnetic resonance imaging; OU, oculus uterque; PosD, possibly damaging; PP, PolyPhen; PrD, probably damaging; PSC, posterior subcapsular cataract; S, SIFT; Tol, tolerated.

* Only one predicted loss-of-function heterozygous variant in an independent exome-based screen of >45,000 individuals was identified (case UK), albeit with a noncolobomatous phenotype.

Variants in *ZFP503* and Human Ocular Disease

To investigate whether variants in *ZFP503* were associated with congenital eye malformations in humans, we sequenced 150 affected individuals with isolated and syndromic optic fissure closure defects from 114 families. Identified variants are shown in the Table. Heterozygous variants from families 107 and 98 were inherited from unaffected/likely unaffected parents and were present in gnomAD at low frequency in European populations (https://gnomad.broadinstitute.org/; family 107, p.Phe222Leu AF = 4.5E-5 or 1 in 36,337; family 98, p.Ala233Pro AF = 4.9E-4 or 1 in 4082 people). These variants did not reach our laboratory's threshold of evidence to be pursued further. The proband in family 107 was also found to have somatic mosaicism for trisomy 20, which may explain his unilateral colobomatous microphthalmia and hemifacial microsomia with hypopigmented skin patches. Affected individuals from these two families also did not harbor potentially pathogenic variants in genes known to cause coloboma in humans (data not shown). We also reviewed data from the United Kingdom's 100,000 Genomes Project.[55] Out of the cohort of approximately 45,000 individuals, one was found to have a clear loss-of-function variant (c. 706G>T, p. Gly24Ter). This 47-year-old woman, however, manifested a retinal dystrophy and no evidence of coloboma. Although the absence of clearly pathogenic variants does not preclude identification of these in other populations, at present we find no association between *ZFP503* coding variants and coloboma in humans.

Discussion

The developmental processes associated with optic fissure closure have been progressively elucidated over the past half century, but the genetics of uveal coloboma is far from well understood. Indeed, two recent studies were only able to molecularly solve approximately 8% to 15% of anophthalmia, microphthalmia, and coloboma cases, consistent with our own laboratory's experience.[8,56,57] Higher yields for molecular testing have been noted in patients with a clearly defined syndrome.[58] In an effort to identify candidate genes for human coloboma, we previously performed developmental profiling of optic fissure closure in mouse,[9] a technique that others have repeated and expanded upon in mouse, chick, and zebrafish in more recent years.[59–62] Here, we show that one gene identified through our screen, *Zfp503*, when knocked out in mouse, produced a uveal coloboma associated with failure of the maintenance of RPE fate. We molecularly characterized this phenotype, showing reduced expression of critical RPE transcription factors such as MITF and OTX2 and the appearance of a neural-retina marker, VSX2, in the proximo-ventral region of the pRPE, accompanied by hyperplasia of cells resembling pNR (Fig. 9).

In mouse, *Zfp503* comprises three exons, of which parts of exons 2 and 3 are protein coding (UCSC browser, GRCm38/mm10). The human ortholog, *ZNF503*, is composed of two exons, both of which include the protein-coding sequence (UCSC browser, GRC38/hg38). A second, noncoding *ZNF503* transcript overlaps only in the first exon. In addition, two long-noncoding RNAs (lncRNAs), *ZNF503-AS1* and *ZNF503-AS2*, each with multiple transcript variants, are present in the most recent human genome assembly. These lncRNAs are not annotated in mouse, nor have we observed them experimentally in total RNA from E11.5 mouse eyes (data not shown). This species difference is important to note, as Chen et al.[63] found that high levels of *ZNF503-AS1*, ergo low *ZNF503* (presumably transcript 1) expression, are correlated with increased RPE differentiation in human, the opposite of what we observed in mouse. The ocular expression pattern of ZFP503 during mouse embryogenesis is largely consistent with earlier studies.[9,18,22] We do note the maintenance of ZFP503 expression throughout the WT embryos even at E12.5 (where mRNA was previously judged low), suggesting the protein may be made earlier and remain stably expressed. Alternatively, the sensitivities of the in situ probes used versus antibody staining after antigen retrieval may be different, resulting in this apparent difference. The positive immunofluorescence signal we observed in fully differentiated mouse retina is consistent with the ganglion cell expression noted in chick by Blixt and colleagues.[16] Although the precise cause of $Zfp503^{-/-}$ neonatal lethality is unclear, expression of *Zfp503* in the developing spinal cord and its role in motor neuron development could explain the atelectasis we noted in the lungs.[12] More recently, Soleilhavoup and colleagues[64] have demonstrated that *Zfp503* is required for proper innervation of the striatum by midbrain dopaminergic neurons in mouse, and its deletion results in a nigral to pallidal lineage conversion and changes in secreted factors in the striatum; thus,

Investigative Ophthalmology & Visual Science

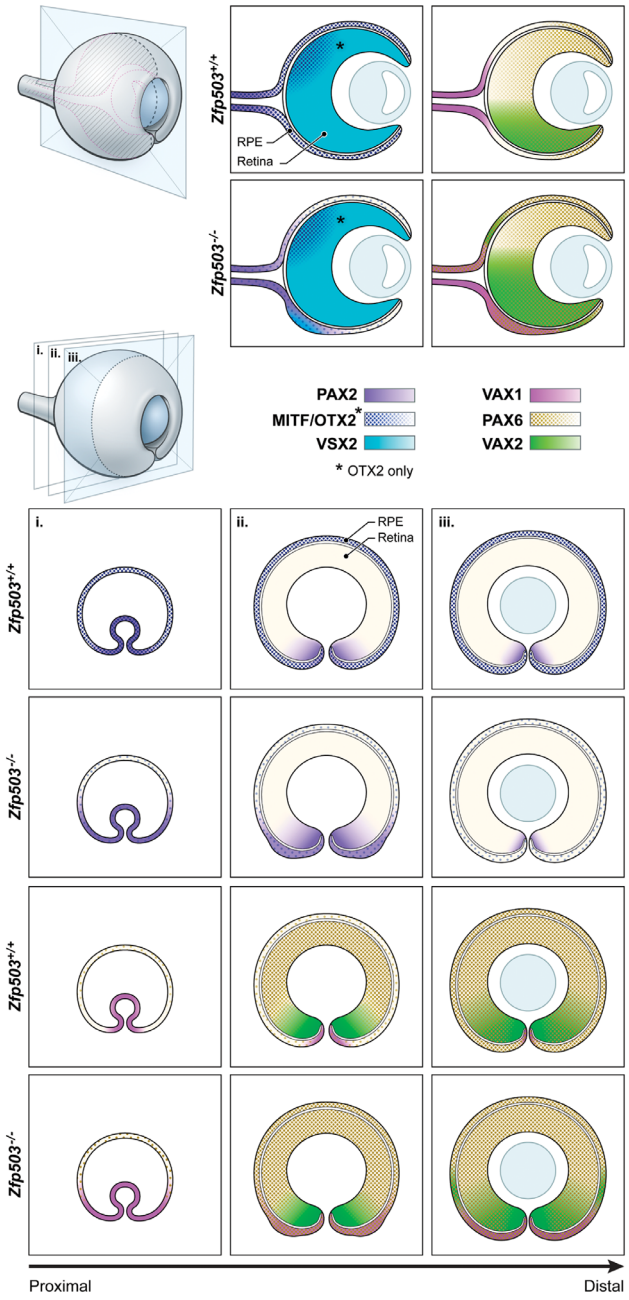

Figure 9. Overview of key transcription factor changes in *Zfp503*$^{-/-}$ embryos. Schematics of coronal (*upper panels*) and sagittal (*lower panels*) sections of mouse embryo eyes around the time of optic fissure closure. Three sagittal sections are shown, proximal to distal from the optic stalk (panels i, ii, and iii, respectively). Reduction in OTX2 and MITF expression is accompanied by abnormal expansions of PAX2, PAX6, *Vax1*, and *Vax2* and the adoption of a neural retina–like phenotype in the pRPE, as evidenced by VSX2 expression. Note that OTX2 and MITF changes in the presumptive RPE are very similar (and shown in one color), with the exception of possible changes in the level of OTX2 in the presumptive neural retina (denoted with an *asterisk*).

we hypothesize that a developmental brain defect could contribute to perinatal lethality.

Published reports suggest that ZFP503 acts as a transcriptional repressor in vitro, likely through interactions with histone deacetylases and corepressor proteins such as members of the GROUCHO family and/or ZBTB32.[9,12–14,17] The patterns of increased expression of PAX6, PAX2, *Vax2*, and *Vax1* in *Zfp503*$^{-/-}$ pRPE are consistent with ZFP503 acting, either directly or indirectly, as a negative regulator of their expression (Fig. 9). Notably, in breast tissue, increased ZFP503 expression results in mammary epithelial cell proliferation and a more highly invasive phenotype by downregulating E-cadherin and GATA3 expression.[13,14]

Loss of MITF expression itself can lead to respecification but in the dorsal, not ventral, portion of the OC.[65] A similar phenotype mediated by an MITF- and OTX2-dependent mechanism is observed when β-catenin is conditionally knocked out in RPE, at least in the early stages of development.[66] In the ventral pRPE, expression of the homeobox genes *Vax1* and *Vax2* is abnormally retained in the absence of MITF.[32] Furthermore, in a triple knockout model (*Mitf/Vax1/Vax2*) where one copy of a *Vax* gene remains, the proximal ventral pRPE transdifferentiates in a way reminiscent of *Zfp503*$^{-/-}$ embryos, implying that the combined effects of these three transcription factors are necessary for proper ventral RPE differentiation. Our finding of increased *Vax2* and *Vax1* expression in *Zfp503*$^{-/-}$ pRPE is consistent with the abnormal retention of expression seen in the MITF-KO mouse. This pattern, however, suggests that the presumed respecification of ventral pRPE is due to another mechanism than the one observed in the three-gene KOs described by Ou et al.[32]

The combined transcriptional activities of PAX2 and PAX6 are required for RPE determination.[43] Both PAX2 and PAX6 activate the MITF-A promoter element in vitro, and the combined absence of PAX2 and PAX6 significantly reduces MITF expression in the developing OC. The presence of expanded domains of PAX2 and PAX6 in the pRPE of *Zfp503*$^{-/-}$ E12.5 embryos suggests that, at least in the ventral-proximal region, coexpression of these transcription factors may be necessary but not sufficient for RPE fate maintenance.

RNA-seq analysis of *Zfp503*$^{-/-}$ versus WT RPE at E11.5 confirmed several of our phenotypic and molecular findings, including changes in genes important for early eye development (e.g., *MITF*, *OTX2*, *PAX6*, *PAX2*) and downregulation of multiple pigmentation-related genes in the KO (e.g., *Tyr*, *Dct*, *Slc45a2*, *Slc24a5*, *Gpnmb*, *Pmel*, *Gpr143*, *Mlana*, *Mlph*). A few differentially regulated genes are known to cause coloboma/microphthalmia/anophthalmia in humans (e.g., *Smoc1*, *Otx2*, *Atoh7*, *Bmp3*).[50,67–69] We posit that within this gene list lie heretofore incompletely characterized genes that have a role in RPE fate maintenance, pigmentation, and/or optic fissure closure. For example, one of the most significantly downregulated genes in *Zfp503*$^{-/-}$ is *Slc4a5*, an electrogenic sodium bicarbonate cotransporter important in brain development and cerebrospinal fluid creation.[70] *Slc4a5* knockout mice have abnormal photoreceptor and ganglion cell numbers with retinal detachment (which may include retinoschisis) and abnormal ERGs. Importantly, although not noted in the article, *Slc4a5* mutant mice appear to have reduced RPE pigmentation in the light and electron microscopy images presented (see Fig. 8 in Kao et al.[70]). This observation, if confirmed, may have important implications for RPE function (e.g., transport) and for melanosome biogenesis. We also note that multiple genes associated with extracellular matrix (ECM) integrity are downregulated in KO embryos (e.g., *Nid2*, *Lama5*, *Col4a4*, *Col8a1*, *Col8a2*, *Col9a3*, *Col12a1*, *Col15a1*, *Timp3*). Biophysical properties of the ECM are known to influence changes in cell state,[71] and proper dissolution of the basement membrane of the

closing edges of the optic fissure is required for fusion.[31,72] Of these, nidogen, in particular, has been shown to be critical for optic cup morphogenesis in zebrafish.[73]

What role, if any, do germline mutations in *ZNF503* have in human disease? Population-based genome databases suggest that this gene is highly constrained with a "probability of loss-of-function intolerant" (pLI) score of 0.95 and an observed/expected ratio of 0.35 (https://gnomad.broadinstitute.org/), making it a good candidate for human disease. In our screen of coloboma families, we found no plausible variants; in the UK 100,000 Genomes Project, we only identified one case with a clear loss-of-function allele (UK, 706G>T, p. Gly24Ter), who did not have coloboma. We note that *ZFP503* has a second ATG, in frame with the canonical translation start site, that would initiate translation with a methionine at amino acid (aa) 79 and produce a shorter protein isoform. Experimental data on ZFP703 that share 53% homology with ZFP503 strongly suggest that a full-length protein and an N-terminal truncated shorter protein might be the products of *ZFP503*.[19] In that case, the variant in "UK" is predicted to allow translation of the shorter isoform from the internal ATG codon with the potential for a compensatory effect. Whether the variants reported here lead to differences in cell physiology and development awaits further study. Regardless, the percentage of inherited ocular disease caused by pathogenic mutations of *ZNF503* is (at best) very low and, given the high degree of genetic constraint and the phenotype of the KO mouse, we hypothesize that biallelic loss-of-function mutations are likely lethal.

In summary, our data support a role for the transcription factor *Zfp503* in completing the differentiation program of the RPE. In the absence of *Zfp503*, lack of RPE cells at the fissure margin results in failure to close the gap and ensuing coloboma. Based on our expression studies in the postnatal mouse eye, we hypothesize additional roles for *Zfp503* in retinal development and/or homeostasis, affecting subpopulations of cells in the retinal ganglion cell (RGC) layer and in the inner nuclear layer (INL). This hypothesis awaits further experimental testing.

Acknowledgments

Supported by the intramural program at the National Eye Institute, National Institutes of Health (NIH), Bethesda, Maryland (Project EY000469). Badea was supported by UEFISCDI grant PN-III-P4-PCE-2021-0333, Romania. Panman was supported by the Medical Research Council, UK. Moshiri was supported by NIH grant K08 EY027463. Thanks goes to the NEI Histology Core for outstanding technical assistance in preparing H&E slides of mouse eyes. This research was made possible through access to the data and findings generated by the 100,000 Genomes Project. The 100,000 Genomes Project is managed by Genomics England Limited (a wholly owned company of the Department of Health and Social Care). The 100,000 Genomes Project is funded by the National Institute for Health Research and NHS England. The Wellcome Trust, Cancer Research UK, and the Medical Research Council have also funded research infrastructure. The 100,000 Genomes Project uses data provided by patients and collected by the National Health Service as part of their care and support.

Disclosure: **E. Boobalan**, None; **A.H. Thompson**, None; **R.P. Alur**, None; **D.M. McGaughey**, None; **L. Dong**, None; **G. Shih**, None; **E.R. Vieta-Ferrer**, None; **I.F. Onojafe**, None; **V.K. Kalaskar**, None; **G. Arno**, None; A.J. **Lotery**, None; **B. Guan**, None; **C. Bender**, None; **O. Memon**, None; **L. Brinster**, None; **C. Soleilhavoup**, None; **L. Panman**, None; **T.C. Badea**, None; **A. Minella**, None; **A.J. Lopez**, None; **S.M. Thomasy**, None; **A. Moshiri**, None; **D. Blain**, None; **R.B. Hufnagel**, None; **T. Cogliati**, None; **K. Bharti**, None; **B.P. Brooks**, None

References

1. Fuhrmann S. Eye morphogenesis and patterning of the optic vesicle. *Curr Top Dev Biol*. 2010;93:61–84.
2. Patel A, Sowden JC. Genes and pathways in optic fissure closure. *Semin Cell Dev Biol*. 2019;91:55–65.
3. Hero I. The optic fissure in the normal and microphthalmic mouse. *Exp Eye Res*. 1989;49:229–239.
4. Williamson KA, FitzPatrick DR. The genetic architecture of microphthalmia, anophthalmia and coloboma. *Eur J Med Genet*. 2014;57:369–380.
5. Hsu P, Ma A, Wilson M, et al. CHARGE syndrome: a review. *J Paediatr Child Health*. 2014;50:504–511.
6. George A, Cogliati T, Brooks BP. Genetics of syndromic ocular coloboma: CHARGE and COACH syndromes. *Exp Eye Res*. 2020;193:107940.
7. Patel A, Hayward JD, Tailor V, et al. The Oculome panel test: next-generation sequencing to diagnose a diverse range of genetic developmental eye disorders. *Ophthalmology*. 2019;126(6):888–907.
8. Kalaskar VK, Alur RP, Li LK, et al. High-throughput custom capture sequencing identifies novel mutations in coloboma-associated genes: mutation in DNA-binding domain of retinoic acid receptor beta affects nuclear localization causing ocular coloboma. *Hum Mutat*. 2020;41:678–695.
9. Brown JD, Dutta S, Bharti K, et al. Expression profiling during ocular development identifies 2 Nlz genes with a critical role in optic fissure closure. *Proc Natl Acad Sci USA*. 2009;106:1462–1467.
10. Pereira Piedade W, Veith S, Famulski JK. Ubiquitin-mediated proteasome degradation regulates optic fissure fusion. *Biol Open*. 2019;8(6):bio044974.
11. Cheah PY, Meng YB, Yang X, Kimbrell D, Ashburner M, Chia W. The Drosophila l(2)35Ba/nocA gene encodes a putative Zn finger protein involved in the development of the embryonic brain and the adult ocellar structures. *Mol Cell Biol*. 1994;14:1487–1499.
12. Ji S-J, Periz G, Sockanathan S. Nolz1 is induced by retinoid signals and controls motoneuron subtype identity through distinct repressor activities. *Development*. 2009;136:231–240.
13. Shahi P, Slorach EM, Wang C-Y, et al. The transcriptional repressor ZNF503/Zeppo2 promotes mammary epithelial cell proliferation and enhances cell invasion. *J Biol Chem*. 2015;290:3803–3813.
14. Shahi P, Wang C-Y, Lawson DA, et al. ZNF503/Zpo2 drives aggressive breast cancer progression by down-regulation of GATA3 expression. *Proc Natl Acad Sci USA*. 2017;114:201701690.
15. Runko AP, Sagerström CG. Nlz belongs to a family of zinc-finger-containing repressors and controls segmental gene expression in the zebrafish hindbrain. *Dev Biol*. 2003;262:254–267.
16. Blixt M, Konjusha D, Ring H, Hallböök F. Zinc finger gene nolz1 regulates the formation of retinal progenitor cells and suppresses the Lim3/Lhx3 phenotype of retinal bipolar cells in chicken retina. *Dev Dynamics*. 2017;247:630–641.
17. Nakamura M, Runko AP, Sagerstrom CG. A novel subfamily of zinc finger genes involved in embryonic development. *J Cell Biochem*. 2004;93:887–895.
18. Hoyle J, Tang YP, Wiellette EL, Wardle FC, Sive H. nlz Gene family is required for hindbrain patterning in the zebrafish. *Dev Dynamics*. 2004;229:835–846.

Investigative Ophthalmology & Visual Science

19. Runko AP, Sagerström CG. Isolation of nlz2 and characterization of essential domains in Nlz family proteins. *J Biol Chem*. 2004;279:11917–11925.
20. Urbán N, Martín-Ibáñez R, Herranz C, et al. Nolz1 promotes striatal neurogenesis through the regulation of retinoic acid signaling. *Neural Dev.* 2010;5:21.
21. McGlinn E, Richman JM, Metzis V, et al. Expression of the NET family member Zfp503 is regulated by hedgehog and BMP signaling in the limb. *Dev Dynamics*. 2008;237:1172–1182.
22. Chang S, Yan Y-T, Shi Y-L, Liu Y-C, Takahashi H, Liu F-C. Region- and cell type-selective expression of the evolutionarily conserved Nolz-1/zfp503 gene in the developing mouse hindbrain. *Gene Expression Patterns*. 2011;11:525–532.
23. Chang C-W, Tsai C-W, Wang H-F, et al. Identification of a developmentally regulated striatum-enriched zinc-finger gene, Nolz-1, in the mammalian brain. *Proc Natl Acad Sci USA*. 2004;101:2613–2618.
24. Bharti K, Liu W, Csermely T, Bertuzzi S, Arnheiter H. Alternative promoter use in eye development: the complex role and regulation of the transcription factor MITF. *Development*. 2008;135:1169–1178.
25. Rigueur D, Lyons KM. Whole-mount skeletal staining. *Methods Mol Biol*. 2014;1130:113–121.
26. Prasov L, Guan B, Ullah E, et al. Novel TMEM98, MFRP, PRSS56 variants in a large United States high hyperopia and nanophthalmos cohort. *Sci Rep*. 2020;10:19986.
27. Richards S, Aziz N, Bale S, et al. Standards and guidelines for the interpretation of sequence variants: a joint consensus recommendation of the American College of Medical Genetics and Genomics and the Association for Molecular Pathology. *Genet Med*. 2015;17:405–424.
28. Taylor RL, Arno G, Poulter JA, et al. Association of steroid 5alpha-reductase type 3 congenital disorder of glycosylation with early-onset retinal dystrophy. *JAMA Ophthalmol*. 2017;135:339–347.
29. Robinson JT, Thorvaldsdottir H, Winckler W, et al. Integrative genomics viewer. *Nat Biotechnol*. 2011;29:24–26.
30. Eckert P, Knickmeyer MD, Heermann S. In vivo analysis of optic fissure fusion in zebrafish: pioneer cells, basal lamina, hyaloid vessels, and how fissure fusion is affected by BMP. *Int J Mol Sci*. 2020;21(8):2760.
31. Weaver ML, Piedade WP, Meshram NN, Famulski JK. Hyaloid vasculature and mmp2 activity play a role during optic fissure fusion in zebrafish. *Sci Rep*. 2020;10:10136.
32. Ou J, Bharti K, Nodari A, Bertuzzi S, Arnheiter H. Vax1/2 genes counteract Mitf-induced respecification of the retinal pigment epithelium. *PLoS ONE*. 2013;8:e59247.
33. Raviv S, Bharti K, Rencus-Lazar S, et al. PAX6 regulates melanogenesis in the retinal pigmented epithelium through feed-forward regulatory interactions with MITF. *PLoS Genetics*. 2014;10:e1004360.
34. Bharti K, Gasper M, Ou J, et al. A regulatory loop involving PAX6, MITF, and WNT signaling controls retinal pigment epithelium development. *PLoS Genet*. 2012;8:e1002757.
35. Nguyen M, Arnheiter H. Signaling and transcriptional regulation in early mammalian eye development: a link between FGF and MITF. *Development (Cambridge, England)*. 2000;127:3581–3591.
36. Rowan S, Chen CM, Young TL, Fisher DE, Cepko CL. Transdifferentiation of the retina into pigmented cells in ocular retardation mice defines a new function of the homeodomain gene Chx10. *Development*. 2004;131:5139–5152.
37. Westenskow P, Piccolo S, Fuhrmann S. β-Catenin controls differentiation of the retinal pigment epithelium in the mouse optic cup by regulating Mitf and Otx2 expression. *Development*. 2009;136:2505–2510.
38. Westenskow PD, McKean JB, Kubo F, Nakagawa S, Fuhrmann S. Ectopic Mitf in the embryonic chick retina by co-transfection of β-catenin and Otx2. *Invest Ophthalmol Vis Sci*. 2010;51:5328–5335.
39. Martínez-Morales J, Dolez V, Rodrigo I, et al. OTX2 activates the molecular network underlying retina pigment epithelium differentiation. *J Biol Chem*. 2003;278:21721–21731.
40. Hodgkinson CA, Moore KJ, Nakayama A, et al. Mutations at the mouse microphthalmia locus are associated with defects in a gene encoding a novel basic-helix-loop-helix-zipper protein. *Cell*. 1993;74:395–404.
41. Martínez-Morales J, Rodrigo I, Bovolenta P. Eye development: a view from the retina pigmented epithelium. *BioEssays*. 2004;26:766–777.
42. Bovolenta P, Mallamaci A, Briata P, Corte G, Boncinelli E. Implication of OTX2 in pigment epithelium determination and neural retina differentiation. *J Neurosci*. 1997;17:4243–4252.
43. Bäumer N, Marquardt T, Stoykova A, et al. Retinal pigmented epithelium determination requires the redundant activities of Pax2 and Pax6. *Development*. 2003;130:2903–2915.
44. Mui SH, Kim JW, Lemke G, Bertuzzi S. Vax genes ventralize the embryonic eye. *Genes Dev*. 2005;19:1249–1259.
45. Strunnikova NV, Maminishkis A, Barb JJ, et al. Transcriptome analysis and molecular signature of human retinal pigment epithelium. *Hum Mol Genet*. 2010;19:2468–2486.
46. Causeret F, Ensini M, Teissier A, et al. Dbx1-expressing cells are necessary for the survival of the mammalian anterior neural and craniofacial structures. *PLoS One*. 2011;6:e19367.
47. Sapkota D, Chintala H, Wu F, Fliesler SJ, Hu Z, Mu X. Onecut1 and Onecut2 redundantly regulate early retinal cell fates during development. *Proc Natl Acad Sci USA*. 2014;111:E4086–4095.
48. Huang T, Li H, Zhang S, Liu F, Wang D, Xu J. Nrn1 overexpression attenuates retinal ganglion cell apoptosis, promotes axonal regeneration, and improves visual function following optic nerve crush in rats. *J Mol Neurosci*. 2021;71:66–79.
49. Paul V, Tonchev AB, Henningfeld KA, et al. Scratch2 modulates neurogenesis and cell migration through antagonism of bHLH proteins in the developing neocortex. *Cereb Cortex*. 2014;24:754–772.
50. Ragge NK, Brown AG, Poloschek CM, et al. Heterozygous mutations of OTX2 cause severe ocular malformations. *Am J Hum Genet*. 2005;76:1008–1022.
51. Khan K, Logan CV, McKibbin M, et al. Next generation sequencing identifies mutations in Atonal homolog 7 (ATOH7) in families with global eye developmental defects. *Hum Mol Genet* .2012;21:776–783.
52. Dakubo GD, Mazerolle C, Furimsky M, et al. Indian hedgehog signaling from endothelial cells is required for sclera and retinal pigment epithelium development in the mouse eye. *Dev Biol*. 2008;320:242–255.
53. Zhou Y, Williams J, Smallwood PM, Nathans J. Sox7, Sox17, and Sox18 cooperatively regulate vascular development in the mouse retina. *PLoS One*. 2015;10:e0143650.
54. Pauls S, Smith SF, Elgar G. Lens development depends on a pair of highly conserved Sox21 regulatory elements. *Dev Biol*. 2012;365:310–318.
55. The National Genomics Research and Healthcare Knowledgebase v5, Genomics England. 2019, doi:10.6084/m9.figshare.4530893.v5.
56. Patel A, Hayward JD, Tailor V, et al. The Oculome Panel Test: next-generation sequencing to diagnose a diverse range of genetic developmental eye disorders. *Ophthalmology*. 2019;126:888–907.

Investigative Ophthalmology & Visual Science

57. Jackson D, Malka S, Harding P, Palma J, Dunbar H, Moosajee M. Molecular diagnostic challenges for non-retinal developmental eye disorders in the United Kingdom. *Am J Med Genet C Semin Med Genet*. 2020;184(3):578–589.
58. ALSomiry AS, Gregory-Evans CY, Gregory-Evans K. An update on the genetics of ocular coloboma. *Hum Genet*. 2019;138(8–9):865–880, doi:10.1007/s00439-019-02019-3.
59. Cao M, Ouyang J, Liang H, et al. Regional gene expression profile comparison reveals the unique transcriptome of the optic fissure. *Invest Ophthalmol Vis Sci*. 2018;59:5773–5784.
60. Hardy H, Prendergast JG, Patel A, et al. Detailed analysis of chick optic fissure closure reveals Netrin-1 as an essential mediator of epithelial fusion. *Elife*. 2019;8:e43877.
61. Richardson R, Owen N, Toms M, Young RM, Tracey-White D, Moosajee M. Transcriptome profiling of zebrafish optic fissure fusion. *Sci Rep*. 2019;9:1541.
62. Patel A, Anderson G, Galea GL, Balys M, Sowden JC. A molecular and cellular analysis of human embryonic optic fissure closure related to the eye malformation coloboma. *Development*. 2020;147(24):dev193649.
63. Chen X, Jiang C, Qin B, et al. LncRNA ZNF503-AS1 promotes RPE differentiation by downregulating ZNF503 expression. *Cell Death Dis*. 2017;8:e3046.
64. Soleilhavoup C, Travaglio M, Patrick K, et al. Nolz1 expression is required in dopaminergic axon guidance and striatal innervation. *Nat Commun*. 2020;11:3111.
65. Bumsted KM, Barnstable CJ. Dorsal retinal pigment epithelium differentiates as neural retina in the microphthalmia (mi/mi) mouse. *Invest Ophthalmol Vis Sci*. 2000;41:903–908.
66. Westenskow P, Piccolo S, Fuhrmann S. Beta-catenin controls differentiation of the retinal pigment epithelium in the mouse optic cup by regulating Mitf and Otx2 expression. *Development*. 2009;136:2505–2510.
67. Okada I, Hamanoue H, Terada K, et al. SMOC1 is essential for ocular and limb development in humans and mice. *Am J Hum Genet*. 2011;88:30–41.
68. Ghiasvand NM, Rudolph DD, Mashayekhi M, JAt Brzezinski, Goldman D, Glaser T. Deletion of a remote enhancer near ATOH7 disrupts retinal neurogenesis, causing NCRNA disease. *Nat Neurosci*. 2011;14:578–586.
69. Fox SC, Widen SA, Asai-Coakwell M, et al. BMP3 is a novel locus involved in the causality of ocular coloboma. *Hum Genet*. 2022;141(8):1385–1407.
70. Kao L, Kurtz LM, Shao X, et al. Severe neurologic impairment in mice with targeted disruption of the electrogenic sodium bicarbonate cotransporter NBCe2 (Slc4a5 gene). *J Biol Chem*. 2011;286:32563–32574.
71. Greenburg G, Hay ED. Cytoskeleton and thyroglobulin expression change during transformation of thyroid epithelium to mesenchyme-like cells. *Development*. 1988;102:605–622.
72. Chan BHC, Moosajee M, Rainger J. Closing the gap: mechanisms of epithelial fusion during optic fissure closure. *Front Cell Dev Biol*. 2020;8:620774.
73. Bryan CD, Casey MA, Pfeiffer RL, Jones BW, Kwan KM. Optic cup morphogenesis requires neural crest-mediated basement membrane assembly. *Development*. 2020;147(4):dev181420.

Investigative Ophthalmology & Visual Science